A drought stress-responsive metabolite malate modulates stomatal responses through G-protein-dependent pathway in grapevine and Arabidopsis

Yoshiharu Mimata[1], Ruhai Gong[1,2], Xuanxuan Pei[1], Guochen Qin[1], Wenxiu Ye[1*]

[1]Peking University Institute of Advanced Agricultural Sciences, Shandong Laboratory of Advanced Agricultural Sciences in Weifang, Shandong 261325, China

[2]College of Horticulture, Shanxi Agricultural University, Shanxi 030801, China

Author for correspondence:

Wenxiu Ye

Tel: +86 5366030821

Email: wenxiu.ye@pku-iaas.edu.cn

Running title: TCA cycle metabolites elicit guard cell signaling

Yoshiharu Mimata: yoshiharu.mimata@pku-iaas.edu.cn

Ruhai Gong: z20223334@stu.sxau.edu.cn

Xuanxuan Pei: xuanxuan.pei@pku-iaas.edu.cn

Guochen Qin: guochen.qin@pku-iaas.edu.cn

Wenxiu Ye: wenxiu.ye@pku-iaas.edu.cn

Abstract

Drought stress is a significant environmental threat to global agricultural production and distribution. Plant adaptation to dehydration stress involves intricate biological processes with substantial changes in metabolite composition. In this study, we investigated the role of tricarboxylic acid (TCA) cycle metabolites in drought tolerance in grapevine and Arabidopsis by metabolome, live cell imaging, electrophysiological and pharmacological approaches. Metabolome analysis revealed that amount of malate, citrate, and isocitrate increased over time in detached grapevine leaves. Ca^{2+} imaging and ion channel measurements indicated that fumarate, malate, and α-ketoglutarate induced cytosolic free Ca^{2+} concentration ($[Ca^{2+}]_{cyt}$) elevation in guard cells and directly activated a guard-cell anion channel SLAC1. However, only malate induced stomatal closure, which required increases in $[Ca^{2+}]_{cyt}$ in guard cells and activation of SLAC1. Through pharmacological experiments and reverse genetics analyses, G-proteins were identified as essential components of malate signaling by regulating second messenger production. These results indicate that TCA cycle metabolites are sensed individually by guard cells and that malate plays a key role in connecting metabolic regulation and drought tolerance through G-protein-dependent signal cascades.

Introduction

Grapevine (*Vitis*) is one of the oldest domesticated crops and holds crucial economic importance for industries through the production of wine, brandy, juice, table grapes, and raisins. Despite the increasing demand for grapes and grape products, the global vineyard area is diminishing annually. In 2023, wine production was anticipated to reach its lowest levels in 60 years, primarily due to the impacts of global climate change (http://www.oiv.int/). Drought constitutes a major environmental stress with global implications for crop survival and yields. The regulation of metabolism stands out as a key mechanism for maintaining cell osmotic potential during drought stress. The metabolic responses to dehydration stress has been comprehensively studied in *Arabidopsis thaliana*. The metabolic reprogramming triggered by drought leads to elevated tricarboxylic acid (TCA) cycle intermediates in leaves (Urano et al., 2009; Pires et al., 2016). TCA cycle intermediates play an essential role in providing energy fuels and metabolic precursors. Malate is crucial due to its significant associations with stomatal movements, aluminum toxicity, CO_2 fixation, ripening, and the taste of berries. Particularly in grapevines, malate is instrumental in determining wine quality and facilitating the growth of microorganisms for vinification (Fernie and Martinoia, 2009; Sweetman et al., 2009). The accumulation of malate is induced by environmental changes and may be linked to physiological responses in various tissues such as leaves, xylem, roots, and mesocarp (Van Kirk and Raschke, 1978; Kondo and Murata, 1987; Delhaize et al., 1993; Hedrich et al., 1994; Patonnier, 1999; Wada et al., 2008; Malcheska et al., 2017). However, the regulatory mechanism of physiological responses by TCA cycle metabolites remains unclear.

In response to drought, plants synthesize a phytohormone abscisic acid (ABA) and close stomatal pores, formed by pairs of guard cells in the epidermis of leaves, to prevent excessive water loss through guard

cell signaling (Hetherington and Woodward, 2003; Murata et al., 2015). Stomatal closure is initiated by the transport of anions across the plasma membrane of guard cells through the slow-type anion channel encoded by the *SLOW ANION CHANNEL-ASSOCIATED 1* (*SLAC1*) gene (Schroeder et al., 2001; Negi et al., 2008; Vahisalu et al., 2008). In ABA signaling, SLAC1 is phosphorylated and activated by cytosolic Ca^{2+} sensor kinases, CALCIUM-DEPENDENT PROTEIN KINASEs (CDPKs) (Brandt et al., 2015), and a Ca^{2+}-independent protein kinase OPEN STOMATA1 (OST1) (Geiger et al., 2009), leading to a decrease in turgor pressure and subsequent stomatal closure. Cytosolic free Ca^{2+} acts as a ubiquitous second messenger, and its concentration transiently increases in response to environmental, developmental, and growth signals (Luan and Wang, 2021). The increase in cytosolic free Ca^{2+} concentration ($[Ca^{2+}]_{cyt}$) results from the uptake of Ca^{2+} into the cell and the release of Ca^{2+} from internal stores through Ca^{2+} channels in response to a membrane potential shift (Hamilton et al., 2000) and second messengers such as cyclic adenosine diphosphate ribose (cADPR) (Leckie et al., 1998), cyclic adenosine monophosphate (cAMP) (Lemtiri-Chlieh and Berkowitz, 2004), inositol trisphosphate (IP_3) (Gilroy et al., 1990), reactive oxygen species (ROS) (Pei et al., 2000), nitric oxide (NO) (Garcia-Mata et al., 2003), cyclic guanosine monophosphate (cGMP) (Wang et al., 2013), and nicotinic acid adenine dinucleotide phosphate (NAADP) (Navazio et al., 2000). In guard cells, cytosolic Ca^{2+} binds to the EF hands of CDPKs, leading to activation of CDPKs, which then induces stomatal closure through the phosphorylation of SLAC1 (Brandt et al., 2015).

Heterotrimeric G-proteins, composed of Gα, Gβ, and Gγ subunits, play pivotal roles in the generation of second messengers, such as cADPR, cAMP, IP_3, and ROS (Zhang et al., 2011; Jin et al., 2013), thereby participating in various biological processes such as growth, development, and responses to environmental stimuli (Jin et al., 2013; Pandey, 2020). The genome of *A. thaliana* encodes one canonical

Gα (GPA1), one Gβ (AGB1), and three Gγ subunits (AGG1–AGG3). GPA1 and/or AGB1 are involved in activating Ca^{2+} channels, slow-type anion channels and K^+ channels and regulating stomatal movements by controlling the production of second messengers in ABA and Ca^{2+} signaling of guard cells (Wang et al., 2001; Fan et al., 2008; Zhang et al., 2011; Jeon et al., 2019). Recent findings have demonstrated that TCA cycle intermediates modulate systemic energy metabolism as metabolic signals "metabokine" *via* G-protein signaling cascades (Krzak et al., 2021). Malate as well as succinate directly binds to a G-protein-coupled receptor (GPCR) and causes rapid increases in $[Ca^{2+}]_{cyt}$ and IP_3 accumulation (Trauelsen et al., 2017). However, it is unknown whether TCA cycle metabolites regulate G-protein signaling in plants.

In this study, we demonstrate that several TCA cycle metabolites accumulate in grapevine leaves during dehydration stress, among which malate most effectively regulates stomatal response *via* a G-protein signaling cascade. We propose that malate forms a hub between energy homeostasis and stress response.

Results

Metabolic responses of TCA cycle metabolites to dehydration stress in grapevine leaves

To investigate metabolic changes in response to drought, grapevine (*Vitis vinifera*) leaves were subjected to water-deficit stress. Detached leaves were sampled at 0–24 h of the dehydration stress treatment and subjected to non-targeted metabolome analysis. Principal component analysis (PCA) revealed that metabolite level changes were not pronounced between 0 and 1 h but gradually increased thereafter (Fig. **1A**). Significant metabolite changes were classified into three patterns: gradual decrease (subclass 1),

gradual increase (subclass 2), and increase followed by decrease (subclass 3) (Supplementary Fig. **S1A**). The endogenous level of a phytohormone abscisic acid (ABA), an indicator of drought stress, increased after 2 h of dehydration stress and reached a plateau after 6 h (Fig. **1B**). After 24 h of treatment, out of 2,407 metabolites, 436 were upregulated, and 80 were downregulated (Fig. **1C**, Supplementary Table **S1**). Amino acids, lipids, terpenoids, phenolic acids, alkaloids, and flavonoids were the primary categories exhibiting changes (Fig. **1D**, Supplementary Fig. **S1B**). Among the upregulated metabolites, we specifically examined three TCA cycle metabolites—malate, isocitrate, and citrate—since malate functions as a signaling molecule inducing stomatal closure in *A. thaliana* (Mimata et al., 2022b). Malate, isocitrate, and citrate increased after 12 or 24 h of dehydration stress (Fig. **1E**). In contrast, *cis*-aconitate decreased immediately after 2–4 h and then returned to basal values.

Effects of TCA cycle metabolites on the $[Ca^{2+}]_{cyt}$ in guard cells

Since Ca^{2+} is a critical second messenger in guard cell signaling, we investigated the effects of TCA cycle metabolites (succinate, fumarate, malate, oxalacetate, α-ketoglutarate, citrate, *cis*-aconitate and isocitrate) and their associated compounds (acetate and pyruvate) on the elevations of $[Ca^{2+}]_{cyt}$ through live cell imaging of *A. thaliana* guard cells expressing a Ca^{2+} sensor fluorescent protein Yellow Cameleon 3.6. Exogenous application of fumarate, malate, α-ketoglutarate, acetate, and pyruvate induced elevations in $[Ca^{2+}]_{cyt}$, significantly increasing the frequency of $[Ca^{2+}]_{cyt}$ elevation compared to mock (Fig. **2**). This finding suggests that α-hydroxy or α-keto acids are effective in $[Ca^{2+}]_{cyt}$ elevation. Here, acetate caused transient long-term $[Ca^{2+}]_{cyt}$ increase (Fig. **2A**). Unlike the normal function of YC3.6, the CFP fluorescence did not return to its baseline, and the YFP fluorescence dropped below the basal level (Supplementary Fig. **S2)**. This dysfunctional response of YC3.6 following the Ca^{2+} surge

125 served as an indicator of impending cell death (Ye et al., 2020). The Ca^{2+} channel blocker La^{3+}
126 completely suppressed the malate-induced $[Ca^{2+}]_{cyt}$ increases (Fig. **2A, D**), indicating that Ca^{2+} channels
127 are responsible for this Ca^{2+} response.

128 **Effects of TCA cycle metabolites on the activation of SLAC1 expressed in Xenopus oocytes**

129 The activation of the SLAC1 anion channel plays a critical role in stomatal closure. VvSLAC1 and
130 AtSLAC1 share 71% amino acid identity. A phenylalanine residue essential for pore gating (F450 in
131 AtSLAC1) is conserved as F440 in VvSLAC1 (Qin et al., 2024). We predicted the structure of
132 VvSLAC1 using *in silico* modeling. The modeling results showed that VvSLAC1 has ten
133 transmembrane helices (Fig. **3 A–D**). The pore is surrounded by an odd number of transmembrane
134 helices and is occluded by F440. To further analyze VvSLAC1 activity, we conducted two-electrode
135 voltage-clamp experiments on Xenopus oocytes. The negative currents in oocytes expressing VvSLAC1
136 were minimal, whereas those in oocytes expressing the VvSLAC1F440A mutant were much higher (Fig.
137 **3E–G**). This indicates that VvSLAC1 is in an inactive state, while VvSLAC1F440A is constitutively
138 active. This finding aligns with previous reports showing that an open-gate mutant, AtSLAC1F450A,
139 exhibits substantial basal activity (Chen et al., 2010). The reversal potential was near the calculated
140 equilibrium potential of Cl^- (approximately 50–80 mV), suggesting that VvSLAC1 permeates Cl^- and
141 that these currents are minimally affected by leak currents.

142 The activity of AtSLAC1F450A is enhanced by malate, whereas that of the wild-type AtSLAC1 is not
143 (Mimata et al., 2022b). To examine the effects of TCA cycle metabolites, VvSLAC1 activity was
144 continuously monitored during perfusion with a bathing solution supplemented with the metabolites.
145 Isocitrate and citrate increased the negative currents in water-injected oocytes (Fig. **4A, B**), indicating

that this activation is due to Xenopus endogenous transporters. None of the other tested metabolites affected the activity of wild-type VvSLAC1 (Fig. **4C, D**). Dicarboxylates, however, promoted the activity of VvSLAC1F440A. These results indicate that the open state of VvSLAC1 is a prerequisite for the promotion of its activity by TCA cycle metabolites. Next, we examined whether these effects depend on membrane potential. The increase in current magnitude was greater as the membrane potential became more negative (Fig. **4E, F**). Excluding oxalacetate, dicarboxylates significantly enhanced VvSLAC1 activity without affecting its reversal potential. These results show that dicarboxylates in the TCA cycle primarily promote Cl^- transport through SLAC1 once it is in the active state.

Malate emerges as a specific modulator in the regulation of stomatal responses

To assess how TCA cycle metabolites influence plant responses to drought stress, we measured stomatal aperture in the presence of the metabolites. After stomata were fully open under light, each metabolite was applied, and stomatal aperture was measured. A significant reduction in stomatal aperture was observed exclusively with malate treatment in *V. vinifera* (Fig. **5A**). Consistent results were obtained using *A. thaliana* (Fig. **5B**). These findings suggest that malate specifically acts as a modulator of stomatal closure.

To further investigate the malate signaling pathway, we conducted a series of pharmacological experiments (Supplementary Table **S2**). We applied anion channel blockers, DIDS and 9-anthracenecarboxylic acid (9-AC) (Schwartz et al., 1995; Geiger et al., 2009), extracellular Ca^{2+} chelator 1,2-bis(2-aminophenoxy)ethane-*N*,*N*,*N*′,*N*′-tetraacetic acid (BAPTA) (Levchenko et al., 2005), and Ca^{2+} channel blockers, nifedipine and La^{3+} (Reiss and Herth, 1985; Pei et al., 2000). Malate-induced stomatal closure in both *V. vinifera* and *A. thaliana* was abolished by all inhibitors (Fig. **5C–F**; Mimata *et al.*,

2022b). These results suggest anion channels and Ca^{2+} signaling *via* Ca^{2+} channels are essential for malate-induced stomatal closure in *V. vinifera* and *A. thaliana*, consistent with the results for $[Ca^{2+}]_{cyt}$ and SLAC1 activity (Fig. **2A, D**, **4D–F**; Mimata *et al.*, 2022b).

Malate stimulates Ca^{2+} signaling *via* second messengers including cADPR, cAMP, and IP_3

To further elucidate the malate-induced stomatal closure, the involvement of second messengers relevant to Ca^{2+} signaling, including cADPR, cAMP, IP_3, ROS, NO, cGMP, NAADP, and PIP_3, was investigated by a pharmacological approach. We applied inhibitors targeting these second messengers that are well-established in plant studies. Nicotinamide, alloxan, neomycin, and salicylhydroxamic acid (SHAM), which are inhibitors of cADPR (Dodd et al., 2007), cAMP (Ma et al., 2009), IP_3 (Tang et al., 2007), and peroxidase-catalyzed ROS production (Mori et al., 2001), respectively, completely abolished the malate-induced stomatal closure in *V. vinifera* and *A. thaliana* (Fig. **4C**, **D**, **F–I**). On the other hand, *N*-nitro-L-arginine methyl ester (L-NAME), 2-(4-carboxyphenyl)-4,4,5,5-tetramethylimidazoline-1-oxyl-3-oxide (cPTIO), LY83583, Ned 19, and wortmannin, which are an NO synthetase inhibitor (Joudoi et al., 2013), an NO scavenger (Isner et al., 2019), a guanylate cyclase inhibitor, an antagonist of NAADP (González et al., 2012), and an inhibitor of PIP_3 production (Matsuoka et al., 1995), respectively, have little inhibitory effect on malate-induced stomatal closure (Supplementary Fig. **S3**). Ca^{2+} imaging experiments further showed that nicotinamide, alloxan, and neomycin but not SHAM inhibited malate-induced $[Ca^{2+}]_{cyt}$ oscillations in Arabidopsis (Fig. **6A, B**). These results suggest that Ca^{2+} signaling involving cADPR, cAMP, and IP_3 is required for malate-induced stomatal closure.

G-proteins are master regulators in malate signaling

Since the generation of cADPR, cAMP, IP_3, and ROS is regulated by G-proteins, their roles in the

stomatal response to malate were investigated with the G-protein inhibitors. All inhibitors completely abolished the malate effect in *V. vinifera* and *A. thaliana* (Fig. **7A**, **B,** Supplementary Fig. **S3E, F**). To confirm the pharmacological result, a reverse genetic approach was performed using loss-of-function mutants for the Gα subunit and Gβ subunit, *gpa1* and *agb1*. The stomata of *gpa1* and *agb1* mutants were insensitive to malate (Fig. **7C**). GDPβS also suppressed malate-induced $[Ca^{2+}]_{cyt}$ elevations and ROS production (Fig. **7D–F**). Furthermore, ROS production was not promoted by malate in the *gpa1* and *agb1* mutants (Fig. **7G**). These data together demonstrate that malate signaling is transduced by G-proteins in guard cells.

Discussion

Drought has severe impacts on agricultural crops and results in metabolite fluctuations in plants. In this study, we identified 436 upregulated and 80 downregulated metabolites in grapevine leaves in response to dehydration stress (Fig. **1C**). These included modulators of stomatal movements, such as phytohormones, primary metabolites, and aromatic secondary metabolites (Supplementary Table **S1**). Among the upregulated metabolites, there were those that induce stomatal closure or inhibit stomatal opening, such as ABA, phaseic acid, adenosine-3'-5'-diphosphate, γ-aminobutyric acid (GABA), and malic acid. On the other hand, among the downregulated metabolites, there were those that promote stomatal opening or inhibit stomatal closure, such as indole-3-acetic acid and 5-aminolevulinic acid. Amino acids and TCA cycle metabolites are osmolytes and their accumulation reduces the water potential. Several amino acids induce stomatal closure through a pathway dependent on glutamate receptor-like channels (GLRs) (Kong et al., 2016). Although TCA cycle metabolites, especially malate, are key metabolites for stomatal movements, their role in signal transduction has remained largely

unknown. This study specifically focused on the effect of TCA cycle metabolites and clarified the mechanism underlying stomatal closure triggered by TCA cycle metabolites.

Specific guard cell responses triggered by TCA cycle metabolites

TCA cycle metabolites elicit distinct guard cell responses, including increases in $[Ca^{2+}]_{cyt}$, activation of SLAC1, and stomatal closure (Fig. **2, 4, 5**). The different specificity of the Ca^{2+} response to TCA cycle metabolites (Fig. **2**), compared to SLAC1 activation (Fig. **4**), suggests that SLAC1 activation does not necessarily lead to increases in $[Ca^{2+}]_{cyt}$, and a carboxylate receptor independent from SLAC1 may exist. Despite both α-ketoglutarate and oxaloacetate are α-keto acids, only α-ketoglutarate, with a carbon chain length similar to glutamate, was effective in inducing elevation of $[Ca^{2+}]_{cyt}$ (Fig. **2A, D**), indicating the importance of carbon chain length in perception. It was shown that dicarboxylate glutamate induces $[Ca^{2+}]_{cyt}$ elevation in guard cells and stomatal closure through a pathway dependent on glutamate receptor-like channels (GLRs), while malate signaling is independently of GLRs (Mimata et al., 2022b). It is plausible that α-ketoglutarate is recognized by GLRs. Even though fumarate and α-ketoglutarate caused Ca^{2+} elevation, SLAC1 activation, and ROS production (Fig. **2A**, **D**, **4,** Supplementary Fig. **S4A**), they failed to close the stomata (Fig. **5A, B**). An unknown factor specific to malate, but not to fumarate or α-ketoglutarate, likely contributes to this process and requires further investigation. Taken together, TCA cycle metabolites are individually sensed by guard cells through distinct mechanisms (Fig. **2, 4, 5**).

Malate plays a key role in stress responses

Dehydration stress initiated the accumulation of ABA after 2 h (Fig. **1B**), which correlates with the onset of stomata closure (Hopper et al., 2014). The endogenous level of malate increased 12 h after dehydration stress (Fig. **1E**). Supporting this, a related study reported 6.78-fold increase in the relative

abundance of malate in Arabidopsis aerial parts after 10 h of dehydration stress (Urano et al., 2009). These findings showed that malate slowly accumulates in whole leaves. Malate was observed to be secreted during stomatal closure (Van Kirk and Raschke, 1978), with its content in guard cells decreasing right after ABA treatment (Kondo and Murata, 1987; Jin et al., 2013). Consistent with these reports, the concentration of apoplast malate increased within 15 minutes in response to elevated CO_2, which triggered stomatal closure (Hedrich et al., 1994). The apoplastic malate concentration is estimated to reach approximately 10 mM, with other metabolites being present in lower concentrations or undetected in leaves of several plant species (Lohaus et al., 1995; Gabriel and Kesselmeier, 1999; Hedrich et al., 2001). Notably, the malate exporter AtALMT12, mainly expressed in guard cells and localized at the plasma membrane, is activated through the ABA signaling pathway (Meyer et al., 2010; Sasaki et al., 2010), and loss-of-function mutation of AtALMT12 has been shown to increase malate content in leaves (Medeiros et al., 2016). These findings suggest that malate is rapidly expelled by transporters and gradually recharged, likely through intracellular biosynthesis, under stress conditions.

Malate was the most potent TCA cycle metabolite that induces stomatal closure (Fig. **5A, B**). The malate-induced stomatal closure has also been confirmed in other methods: feeding malate through the petiole decreases stomatal aperture and conductance in ash and aspen trees (Patonnier, 1999; Rasulov et al., 2018). The *atalmt12* mutants exhibit increased malate accumulation and weaker and slower stomatal closure in leaves (Meyer et al., 2010; Sasaki et al., 2010; Medeiros et al., 2016). As AtALMT12 is gated by malate (Meyer et al., 2010), exported malate accelerates malate efflux as a feedback loop. This process subsequently leads to malate accumulation in apoplast, which activates SLAC1 and drives stomatal closure. Moreover, exogenous application of malate inhibits stomatal opening (Esser et al., 1997). Therefore, malate may play a role in maintaining stomatal closure to reduce water loss and

enhance drought tolerance. This hypothesis is further supported by a report showing that *atalmt12* mutants are sensitive to drought stress (Medeiros et al., 2016).

Malate signaling is mediated by a specific set of second messengers

Stomatal measurements (Fig. **5D, G)** and Ca^{2+} imaging (Fig. **6**) with inhibitors suggest the involvement of second messengers including cAMP, cADPR, and IP_3 in malate signaling. cAMP triggers Ca^{2+} influx through CYCLIC NUCLEOTIDE-GATED CHANNELS (CNGCs) in guard cells (Lemtiri-Chlieh and Berkowitz, 2004; Ali et al., 2007). Recently, it was reported that multiple CNGCs work redundantly as ABA-activated Ca^{2+} channels, which are necessary for ABA-induced Ca^{2+} oscillations and stomatal closure independently of ROS (Tan et al., 2023; Yang et al., 2024). Future studies should investigate the involvement of CNGCs in malate signaling.

Malate-induced stomatal closure required the peroxidase activity (Fig. **5H, I**). Malate promotes ROS production by peroxidases (Mimata et al., 2022a), and ROS increase $[Ca^{2+}]_{cyt}$ *via* plasma membrane Ca^{2+} channels (Pei et al., 2000). Based on these observations, we hypothesized that malate accelerates Ca^{2+} influx by promoting ROS production. Contrary to our hypothesis, the inhibition of ROS production did not impair malate-induced Ca^{2+} responses (Fig. **6**). Moreover, blocking Ca^{2+} influx did not affect ROS production (Supplementary Fig. **S4B**). These findings indicate that ROS production is independent of Ca^{2+} signaling in malate-induced stomatal closure.

Malate signaling is transduced by G-protein signaling cascades

In mammals, carboxylates, such as succinate and malate, are sensed by a GPCR. Succinate is released from stimulated macrophages and injured tissues, reaching millimolar concentrations locally

(Chouchani et al., 2014; Littlewood-Evans et al., 2016). Extracellular succinate activates GPCRs, stimulating IP_3 formation, inhibiting cAMP production, and increasing $[Ca^{2+}]_{cyt}$ *via* the G-protein signaling pathway (He et al., 2004; Trauelsen et al., 2021). Likewise, malate is recognized by the succinate receptor, leading to rapid increases in intracellular $[Ca^{2+}]$ and IP_3 accumulation (Trauelsen et al., 2017).

In this study, pharmacological and reverse genetics experiments demonstrated the involvement of second messengers, such as Ca^{2+}, cAMP, IP_3, and G-proteins, in malate signaling in plants (Fig. **7**). Unlike animal GPCRs, plant GPCRs lack well-characterized guanine nucleotide exchange factor activity, and such GPCRs have not yet been identified. Nevertheless, TCA cycle metabolites are common stress-responsive signal molecules mediated by G-protein-dependent signaling cascades in both animal and plant kingdoms.

Based on our findings, we propose a model summarizing malate signaling in guard cells (Fig. **7H**). The malate signal is transmitted *via* G-proteins, which regulate the generation of second messengers. This signaling cascade induces increases in $[Ca^{2+}]_{cyt}$, which activates SLAC1 through phosphorylation by Ca^{2+}-dependent protein kinases. Consequently, malate promotes Cl^- transport through active-form SLAC1, decreasing turgor pressure and driving stomatal closure.

Materials and Methods

Plants and growth conditions

Grapevine (*V. vinifera* L. cv. Chardonnay) was grown on a soil mixture of 1:1 = soil: vermiculite (v/v)

in a growth room at 24℃ and 80% relative humidity under 16 h-light/8 h-dark photoperiod with a photon flux density of 100 μmol m^{-2} s^{-1}. Arabidopsis (*A. thaliana* L. ecotype Colombia-0) was grown on a soil mixture of 1:1 = soil: vermiculite (v/v) in a growth chamber at 21℃ and 60% relative humidity under 16 h-light/8 h-dark photoperiod with a photon flux density of 120 μmol m^{-2} s^{-1}. The T-DNA insertion lines, *gpa1* (SALK_001846 and SALK_066823C) and *agb1* (SALK_077086C and SALK_204268C), were obtained from Arashare and NASC.

Dehydration stress treatment

Fully expanded leaves from 1 to 2-month-old grapevine plants were randomly detached. Dehydration was performed as described previously (Urano et al., 2009) with a few modifications. The detached leaves were exposed to dehydration stress on the paper at 26℃ and ambient humidity under light. At indicated time, the leaves were frozen by liquid nitrogen.

Sample preparation for LC-MS

The detached leaves were freeze-dried in a lyophilizer (Scientz-100F; Scientz, Zhejiang, China) and then homogenized (30 Hz, 1.5 min) into powder using a grinder (MM 400; Retsch, Dusseldorf, Germany). Next, 1200 μL of -20℃ pre-cooled 70% methanolic aqueous internal standard extract added to 50 mg of sample powder. The sample was vortexed once every 30 min for 30 s, for a total of 6 times. After centrifugation at 12000 rpm for 3 min, the supernatant was aspirated, and the sample was filtered through a microporous membrane (0.22 μm pore size) and stored in the injection vial for UPLC-MS/MS analysis.

Metabolite analysis using LC-MS

The sample extracts were analyzed using an UPLC-ESI-MS/MS system (UPLC, ExionLC™ AD: SCIEX, MA, USA; MS, Applied Biosystems 4500 Q TRAP: SCIEX). The analytical conditions were as follows, UPLC: column, Agilent SB-C18 (1.8 μm, 2.1 mm * 100 mm); The mobile phase was consisted of solvent A, pure water with 0.1% formic acid, and solvent B, acetonitrile with 0.1% formic acid. Sample measurements were performed with a gradient program that employed the starting conditions of 95% A, 5% B. Within 9 min, a linear gradient to 5% A, 95% B was programmed, and a composition of 5% A, 95% B was kept for 1 min. Subsequently, a composition of 95% A, 5.0% B was adjusted within 1.1 min and kept for 2.9 min. The flow velocity was set as 0.35 mL per min; The column oven was set to 40°C; The injection volume was 4 μL. The effluent was alternatively connected to an ESI-triple quadrupole-linear ion trap (QTRAP)-MS.

The ESI source operation parameters were as follows: source temperature 550°C; ion spray voltage (IS) 5500 V (positive ion mode)/-4500 V (negative ion mode); ion source gas I (GSI), gas II (GSII), curtain gas (CUR) were set at 50, 60, and 25 psi, respectively; the collision-activated dissociation (CAD) was high. QQQ scans were acquired as MRM experiments with collision gas (nitrogen) set to medium. DP (declustering potential) and CE (collision energy) for individual MRM transitions was done with further DP and CE optimization. A specific set of MRM transitions were monitored for each period according to the metabolites eluted within this period.

Sample preparation for GC-MS

The leaves subjected dehydration stress were ground to a powder in liquid nitrogen. 500 mg (1 mL) of the powder was transferred immediately to a 20 mL head-space vial (Agilent, CA, USA), containing NaCl saturated solution, to inhibit any enzyme reaction. The vials were sealed using crimp-top caps with

TFE-silicone headspace septa (Agilent). At the time of SPME analysis, each vial was placed in 60℃ for 5 min, then a 120 μm DVB/CWR/PDMS fiber (Agilent) was exposed to the headspace of the sample for 15 min at 60℃.

Metabolite analysis using GC-MS

After sampling, desorption of the VOCs from the fiber coating was carried out in the injection port of the GC apparatus (Model 8890; Agilent) at 250℃ for 5 min in the splitless mode. The identification and quantification of VOCs was carried out using an Agilent Model 8890 GC and a 7000D mass spectrometer (Agilent), equipped with a 30 m × 0.25 mm × 0.25 μm DB-5MS (5% phenyl-polymethylsiloxane) capillary column. Helium was used as the carrier gas at a linear velocity of 1.2 mL/min. The injector temperature was kept at 250℃ and the detector at 280℃. The oven temperature was programmed from 40℃ (3.5 min), increasing at 10℃/min to 100℃, at 7℃/min to 180℃, at 25℃/min to 280℃, hold for 5 min. Mass spectra was recorded in electron impact (EI) ionization mode at 70 eV. The quadrupole mass detector, ion source and transfer line temperatures were set, respectively, at 150, 230 and 280℃. The MS was selected ion monitoring (SIM) mode was used for the identification and quantification of analytes.

Data analysis of the non-target metabolome

Relative metabolite abundances were calculated by the peak areas. Unsupervised PCA was performed by statistics function prcomp within R (www.r-project.org). The relative contents of all differential metabolites were processed by UV (unit variance scaling) followed by K-Means cluster analysis. Identified metabolites were annotated using KEGG Compound database (http://www.kegg.jp/kegg/compound/). Pathways with significantly regulated metabolites mapped to

were then fed into metabolite sets enrichment analysis (MSEA), their significance was determined by hypergeometric test's P-values. Upregulated metabolites are defined VIP >1, $\log_2$ (Fold change) ≥1 and P-value >0.05, downregulated metabolites are defined VIP >1, $\log_2$ (Fold change) ≤−1 and P-value >0.05. P-value was calculated by Welch's t-test.

$[Ca^{2+}]_{cyt}$ imaging

Wild-type Arabidopsis plants expressing Yellow Cameleon 3.6 were used to measure $[Ca^{2+}]_{cyt}$ in guard cells as described previously (Mimata et al., 2022b). The abaxial side of an excised rosette leaf was gently attached to a glass slide with a medical adhesive (stock no. 7730; Hollister, IL, USA) and then mesophyll tissues were whittled away with a razor blade to keep the abaxial epidermis intact on the slide. The remaining abaxial epidermis was immersed in stomatal assay solution, comprising 5 mM KCl, 50 μM $CaCl_2$ and 10 mM MES/Tris (pH 5.6), in the light for 2 h to induce stomatal opening. The epidermis was treated with 10 mM TCA cycle metabolites in stomatal assay solution at the indicated time. Inhibitors were added 5 min before starting imaging. The stock solution of TCA cycle metabolites was dissolved in stomatal assay solution and adjusted to a pH of 5.6 with Tris.

The images were acquired under a fluorescence microscope (ECLIPSE Ti2-E; NIKON). Excitation light was provided by a mercury arc lamp and a 436 nm filter (ET436/20x, Chroma Technology Corporation, VT, USA). Emission of the CFP was measured at 480 nm filter (ET480/40m, Chroma Technology Corporation) and of the YFP at 535 nm filter (ET535/30m, Chroma Technology Corporation) using a CMOS camera (ORCA-Fusion BT Digital CMOS camera C15440; HAMAMATSU, Shizuoka, Japan). Images were taken every 5 s.

Modeling

AlphaFold3 was used to predict the protein structure of VvSLAC1. Five protomer models were generated, with predicted template modeling scores raging from 0.65 to 0.67 and ranking scores raging from 0.81 to 0.83. The models were compared with the cryo-EM structure of AtSLAC1 (PDBs 8gw6: Lee et al., 2023) and the top-scored model has a root mean square deviation of 0.852 Å/335 Cα. Due to the limited length of the AtSLAC1 structure, the residues 1-141 and 507-553 in VvSLAC1 were removed.

Cloning and cRNA synthesis

All constructs were cloned into the oocyte expression vector pNB1u (Nour-Eldin et al., 2006) by ClonExpress II One Step Cloning Kit (Vazyme Biotech, Nanjing, China). The site-directed mutants were generated by FastCloning (Li et al., 2011). VvSLAC1 (LOC100244459) cDNA from *V. vinifera* was used for cloning, and all constructs were verified by sequencing. Primers used for cloning and site-directed mutagenesis are listed in Table S3. cRNA was prepared using an mMESSAGE mMACHINE ™ T7 Transcription Kit (Thermo Fisher Scientific, MA, USA).

Two-electrode voltage-clamp

Xenopus laevis oocytes were injected with 50 nL cRNA (each 10 ng) and incubated in ND96 buffer at 18°C for a few days before voltage-clamp recordings (Mimata et al., 2022b). The bath solution contained 1 mM Mg-gluconate, 1 mM Ca-gluconate and 1 mM $LaCl_3$ ± 10 mM TCA cycle metabolites buffered with 10 mM MES/Tris to adjust the pH to 5.6. Osmolality was adjusted to 220 mOsmol kg^{-1} using D-sorbitol. The voltage pulse was commanded to clamp the membrane potential at −120 mV in gap-free or from +60 to −160 mV in 20 mV decrements in step for 2.5 s with a holding potential of 0 mV. Voltage-clamp recordings for oocytes were performed using an Axoclamp 900A amplifier (Molecular Devices,

CA, USA), data were acquired using a Digidata 1550B system (Molecular Devices) and analyzed using pCLAMP 11.2 software (Molecular Devices).

Measurement of stomatal aperture

Stomatal apertures were measured as described previously (Ye et al., 2020) with modifications. Leaf discs (4 mm in diameter) obtained from fully expanded leaves were placed abaxial side down on stomatal assay solution. The discs were exposed to light for 2 h to induce stomatal opening and subsequently treated with 10 mM TCA cycle metabolites in stomatal assay solution for an additional 2 h. Inhibitors were added 5 min before malate treatment. The types and concentrations of inhibitors are listed in Supplementary Table S2. The abaxial epidermis was captured under optical microscopes (ECLIPSE Ts-2R, ECLIPSE Ti2-E and ECLIPSE Ci; NIKON, Tokyo, Japan) using NIS ELEMENTS software (NIKON). Stomatal apertures were quantified using IMAGEJ software (NIH). We measured 30 stomatal apertures from a leaf disc to calculate an average. This measurement was repeated four times using different plants, and the overall average was calculated.

Measurement of ROS production

ROS production in guard cells was analyzed using the fluorescent dye 2',7'-dihydrodichlorofluorescein diacetate (H_2DCF-DA) as described previously (Mimata et al., 2022a) with modifications. The abaxial side of an excised rosette leaf was gently attached to a glass slide with a medical adhesive and then mesophyll tissues were whittled away with a razor blade. The remaining abaxial epidermis was immersed in stomatal assay solution in the light for 2 h to induce stomatal opening. A total of 50 μM

417 H_2DCF-DA was added to the stomatal assay solution and the epidermal tissues were incubated in the
418 dark for 30 min. After the dye loading, the epidermal tissues were gently rinsed with stomatal assay
419 solution. The epidermis was treated with 10 mM TCA cycle metabolites ± inhibitor in stomatal assay
420 solution. After the 30 min incubation, fluorescent signals were captured using the fluorescence
421 microscope with 480 ± 15 nm/ 535 ± 23 nm excitation/emission filters. We measured 30 guard cells
422 from an epidermis to calculate an average. This measurement was repeated three times using different
423 plants, and the overall average was calculated.
424

425 **Acknowledgements**

426 We thank Dr. Hussam Hassan Nour-Eldin (University of Copenhagen) for providing pNB1u vector; Dr.
427 Yoshiyuki Murata and Dr. Shintaro Munemasa (Okamaya University) for providing plasmid constructs;
428 Dongyue Wang (Peking University Institute of Advanced Agricultural Sciences) for helping cloning.

429 **Funding**

430 This research was supported by Taishan Scholars Program of Shandong Province and Shandong
431 Provincial Science and Technology Innovation Fund.

432 **Authors' contributions**

433 YM and WY planned and designed the research. YM, RG and XP performed experiments. YM analyzed
434 data. YM, GQ and WY interpreted the data. YM and WY wrote the manuscript.

435 **Ethics approval and consent to participate**

436 Not applicable.

437 **Consent for publication**

438 All authors approve the manuscript and consent to the publication of the work.

439 **Competing interests**

440 The authors declare no conflicts of interest.

441 **Availability of data and materials**

442 The datasets during and/or analyzed during the current study available from the corresponding author
443 on reasonable request.

444 **Supplementary information**

445 The following materials are available in the online version of this article.

446 **Supplementary Figure S1.** Metabolome analysis in grapevine leaves during dehydration treatment.

447 **Supplementary Figure S2.** Ca^{2+} response to acetate in guard cells.

448 **Supplementary Figure S3.** Malate-induced stomatal closure in the presence of inhibitors.

449 **Supplementary Figure S4.** ROS production in the presence of TCA cycle metabolites.

450 **Supplementary Table S1.** Dataset of metabolome analysis.

451 **Supplementary Table S2.** List of inhibitors used in this work.

Supplementary Table S3. List of primers used in this work.

References

Ali R, Ma W, Lemtiri-Chlieh F, Tsaltas D, Leng Q, Von Bodman S, Berkowitz GA (2007) Death Don't Have No Mercy and Neither Does Calcium: *Arabidopsis* CYCLIC NUCLEOTIDE GATED CHANNEL2 and Innate Immunity. The Plant Cell **19**: 1081–1095

Brandt B, Munemasa S, Wang C, Nguyen D, Yong T, Yang PG, Poretsky E, Belknap TF, Waadt R, Alemán F, et al (2015) Calcium specificity signaling mechanisms in abscisic acid signal transduction in Arabidopsis guard cells. eLife **4**: e03599

Chen Y, Hu L, Punta M, Bruni R, Hillerich B, Kloss B, Rost B, Love J, Siegelbaum SA, Hendrickson WA (2010) Homologue structure of the SLAC1 anion channel for closing stomata in leaves. Nature **467**: 1074–1080

Chouchani ET, Pell VR, Gaude E, Aksentijević D, Sundier SY, Robb EL, Logan A, Nadtochiy SM, Ord ENJ, Smith AC, et al (2014) Ischaemic accumulation of succinate controls reperfusion injury through mitochondrial ROS. Nature **515**: 431–435

Delhaize E, Ryan PR, Randall PJ (1993) Aluminum Tolerance in Wheat (Triticum aestivum L.) (II. Aluminum-Stimulated Excretion of Malic Acid from Root Apices). Plant Physiol **103**: 695–702

Dodd AN, Gardner MJ, Hotta CT, Hubbard KE, Dalchau N, Love J, Assie J-M, Robertson FC, Jakobsen MK, Gonçalves J, et al (2007) The *Arabidopsis* Circadian Clock Incorporates a cADPR-Based Feedback Loop. Science **318**: 1789–1792

Esser JE, Liao Y-J, Schroeder JI (1997) Characterization of ion channel modulator effects on ABA- and malate-induced stomatal movements: strong regulation by kinase and phosphatase inhibitors, and

relative insensitivity to mastoparans. Journal of Experimental Botany **48**: 539–550

Fan L-M, Zhang W, Chen J-G, Taylor JP, Jones AM, Assmann SM (2008) Abscisic acid regulation of guard-cell K^+ and anion channels in Gβ- and RGS-deficient *Arabidopsis* lines. Proc Natl Acad Sci USA **105**: 8476–8481

Fernie AR, Martinoia E (2009) Malate. Jack of all trades or master of a few? Phytochemistry **70**: 828–832

Gabriel R, Kesselmeier J (1999) Apoplastic Solute Concentrations of Organic Acids and Mineral Nutrients in the Leaves of Several Fagaceae. Plant and Cell Physiology **40**: 604–612

Garcia-Mata C, Gay R, Sokolovski S, Hills A, Lamattina L, Blatt MR (2003) Nitric oxide regulates K^+ and Cl^- channels in guard cells through a subset of abscisic acid-evoked signaling pathways. Proc Natl Acad Sci USA **100**: 11116–11121

Geiger D, Scherzer S, Mumm P, Stange A, Marten I, Bauer H, Ache P, Matschi S, Liese A, Al-Rasheid KAS, et al (2009) Activity of guard cell anion channel SLAC1 is controlled by drought-stress signaling kinase-phosphatase pair. Proc Natl Acad Sci USA **106**: 21425–21430

Gilroy S, Read ND, Trewavas AJ (1990) Elevation of cytoplasmic calcium by caged calcium or caged inositol trisphosphate initiates stomatal closure. Nature **346**: 769–771

González A, Cabrera MDLÁ, Henríquez MJ, Contreras RA, Morales B, Moenne A (2012) Cross Talk among Calcium, Hydrogen Peroxide, and Nitric Oxide and Activation of Gene Expression Involving Calmodulins and Calcium-Dependent Protein Kinases in *Ulva compressa* Exposed to Copper Excess. Plant Physiology **158**: 1451–1462

Hamilton DWA, Hills A, Köhler B, Blatt MR (2000) Ca^{2+} channels at the plasma membrane of stomatal guard cells are activated by hyperpolarization and abscisic acid. Proc Natl Acad Sci USA **97**:

4967–4972

He W, Miao FJ-P, Lin DC-H, Schwandner RT, Wang Z, Gao J, Chen J-L, Tian H, Ling L (2004) Citric acid cycle intermediates as ligands for orphan G-protein-coupled receptors. Nature **429**: 188–193

Hedrich R, Marten I, Lohse G, Dietrich P, Winter H, Lohaus G, Heldt H (1994) Malate-sensitive anion channels enable guard cells to sense changes in the ambient CO_2 concentration. The Plant Journal **6**: 741–748

Hedrich R, Neimanis S, Savchenko G, Felle HH, Kaiser WM, Heber U (2001) Changes in apoplastic pH and membrane potential in leaves in relation to stomatal responses to CO_2, malate, abscisic acid or interruption of water supply. Planta **213**: 594–601

Hetherington AM, Woodward FI (2003) The role of stomata in sensing and driving environmental change. Nature **424**: 901–908

Hopper DW, Ghan R, Cramer GR (2014) A rapid dehydration leaf assay reveals stomatal response differences in grapevine genotypes. Hortic Res **1**: 2

Isner J-C, Olteanu V-A, Hetherington AJ, Coupel-Ledru A, Sun P, Pridgeon AJ, Jones GS, Oates M, Williams TA, Maathuis FJM, et al (2019) Short- and Long-Term Effects of UVA on Arabidopsis Are Mediated by a Novel cGMP Phosphodiesterase. Current Biology **29**: 2580-2585.e4

Jeon BW, Acharya BR, Assmann SM (2019) The Arabidopsis heterotrimeric G-protein β subunit, AGB1, is required for guard cell calcium sensing and calcium-induced calcium release. The Plant Journal **99**: 231–244

Jin X, Wang R-S, Zhu M, Jeon BW, Albert R, Chen S, Assmann SM (2013) Abscisic Acid–Responsive Guard Cell Metabolomes of *Arabidopsis* Wild-Type and *gpa1* G-Protein Mutants. The Plant Cell **25**: 4789–4811

Joudoi T, Shichiri Y, Kamizono N, Akaike T, Sawa T, Yoshitake J, Yamada N, Iwai S (2013) Nitrated Cyclic GMP Modulates Guard Cell Signaling in *Arabidopsis*. The Plant Cell **25**: 558–571

Kondo N, Murata I (1987) Abscisic Acid-Induced Stomatal Closure in Vicia faba Epidermal Strips. Excretion of Solutes from Guard Cells and Increase in Elastic Modulus of Guard Cell Wall. Plant and Cell Physiology **28**: 355–364

Kong D, Hu H-C, Okuma E, Lee Y, Lee HS, Munemasa S, Cho D, Ju C, Pedoeim L, Rodriguez B, et al (2016) L-Met Activates Arabidopsis GLR Ca^{2+} Channels Upstream of ROS Production and Regulates Stomatal Movement. Cell Reports **17**: 2553–2561

Krzak G, Willis CM, Smith JA, Pluchino S, Peruzzotti-Jametti L (2021) Succinate Receptor 1: An Emerging Regulator of Myeloid Cell Function in Inflammation. Trends in Immunology **42**: 45–58

Leckie CP, McAinsh MR, Allen GJ, Sanders D, Hetherington AM (1998) Abscisic acid-induced stomatal closure mediated by cyclic ADP-ribose. Proc Natl Acad Sci USA **95**: 15837–15842

Lee Y, Jeong HS, Jung S, Hwang J, Le CTH, Jun S-H, Du EJ, Kang K, Kim B-G, Lim H-H, et al (2023) Cryo-EM structures of the plant anion channel SLAC1 from Arabidopsis thaliana suggest a combined activation model. Nat Commun **14**: 7345

Lemtiri-Chlieh F, Berkowitz GA (2004) Cyclic Adenosine Monophosphate Regulates Calcium Channels in the Plasma Membrane of Arabidopsis Leaf Guard and Mesophyll Cells. Journal of Biological Chemistry **279**: 35306–35312

Levchenko V, Konrad KR, Dietrich P, Roelfsema MRG, Hedrich R (2005) Cytosolic abscisic acid activates guard cell anion channels without preceding Ca^{2+} signals. Proc Natl Acad Sci USA **102**: 4203–4208

Li C, Wen A, Shen B, Lu J, Huang Y, Chang Y (2011) FastCloning: a highly simplified, purification-

free, sequence- and ligation-independent PCR cloning method. BMC Biotechnol **11**: 92

Littlewood-Evans A, Sarret S, Apfel V, Loesle P, Dawson J, Zhang J, Muller A, Tigani B, Kneuer R, Patel S, et al (2016) GPR91 senses extracellular succinate released from inflammatory macrophages and exacerbates rheumatoid arthritis. Journal of Experimental Medicine **213**: 1655–1662

Lohaus G, Winter H, Riens B, Heldt HW (1995) Further Studies of the Phloem Loading Process in Leaves of Barley and Spinach. The Comparison of Metabolite Concentrations in the Apoplastic Compartment with those in the Cytosolic Compartment and in the Sieve Tubes[1]. Botanica Acta **108**: 270–275

Luan S, Wang C (2021) Calcium Signaling Mechanisms Across Kingdoms. Annu Rev Cell Dev Biol **37**: 311–340

Ma W, Qi Z, Smigel A, Walker RK, Verma R, Berkowitz GA (2009) Ca^{2+}, cAMP, and transduction of non-self perception during plant immune responses. Proc Natl Acad Sci USA **106**: 20995–21000

Malcheska F, Ahmad A, Batool S, Müller HM, Ludwig-Müller J, Kreuzwieser J, Randewig D, Hänsch R, Mendel RR, Hell R, et al (2017) Drought-Enhanced Xylem Sap Sulfate Closes Stomata by Affecting ALMT12 and Guard Cell ABA Synthesis. Plant Physiol **174**: 798–814

Matsuoka K, Bassham DC, Raikhel NV, Nakamura K (1995) Different sensitivity to wortmannin of two vacuolar sorting signals indicates the presence of distinct sorting machineries in tobacco cells. The Journal of cell biology **130**: 1307–1318

Medeiros DB, Martins SCV, Cavalcanti JHF, Daloso DM, Martinoia E, Nunes-Nesi A, DaMatta FM, Fernie AR, Araújo WL (2016) Enhanced Photosynthesis and Growth in *atquac1* Knockout Mutants Are Due to Altered Organic Acid Accumulation and an Increase in Both Stomatal and Mesophyll Conductance. Plant Physiol **170**: 86–101

Meyer S, Mumm P, Imes D, Endler A, Weder B, Al-Rasheid KAS, Geiger D, Marten I, Martinoia E, Hedrich R (2010) AtALMT12 represents an R-type anion channel required for stomatal movement in Arabidopsis guard cells: AtALMT12-mediated release of anions in guard cells. The Plant Journal **63**: 1054–1062

Mimata Y, Munemasa S, Akter F, Jahan I, Nakamura T, Nakamura Y, Murata Y (2022a) Malate induces stomatal closure *via* a receptor-like kinase GHR1- and reactive oxygen species-dependent pathway in *Arabidopsis thaliana*. Bioscience, Biotechnology, and Biochemistry **86**: 1362–1367

Mimata Y, Munemasa S, Nakamura T, Nakamura Y, Murata Y (2022b) Extracellular malate induces stomatal closure via direct activation of guard-cell anion channel SLAC1 and stimulation of Ca2+ signalling. New Phytologist **236**: 852–863

Mori IC, Pinontoan R, Kawano T, Muto S (2001) Involvement of Superoxide Generation in Salicylic Acid-Induced Stomatal Closure in Vicia faba. Plant and Cell Physiology **42**: 1383–1388

Murata Y, Mori IC, Munemasa S (2015) Diverse Stomatal Signaling and the Signal Integration Mechanism. Annu Rev Plant Biol **66**: 369–392

Navazio L, Bewell MA, Siddiqua A, Dickinson GD, Galione A, Sanders D (2000) Calcium release from the endoplasmic reticulum of higher plants elicited by the NADP metabolite nicotinic acid adenine dinucleotide phosphate. Proc Natl Acad Sci USA **97**: 8693–8698

Negi J, Matsuda O, Nagasawa T, Oba Y, Takahashi H, Kawai-Yamada M, Uchimiya H, Hashimoto M, Iba K (2008) CO_2 regulator SLAC1 and its homologues are essential for anion homeostasis in plant cells. Nature **452**: 483–486

Nour-Eldin HH, Hansen BG, Nørholm MHH, Jensen JK, Halkier BA (2006) Advancing uracil-excision based cloning towards an ideal technique for cloning PCR fragments. Nucleic Acids Research

34: e122–e122

Pandey S (2020) Plant receptor-like kinase signaling through heterotrimeric G-proteins. Journal of Experimental Botany **71**: 1742–1751

Patonnier M (1999) Drought-induced increase in xylem malate and mannitol concentrations and closure of Fraxinus excelsior L. stomata. Journal of Experimental Botany **50**: 1223–1231

Pei Z-M, Murata Y, Benning G, Thomine S, Klüsener B, Allen GJ, Grill E, Schroeder JI (2000) Calcium channels activated by hydrogen peroxide mediate abscisic acid signalling in guard cells. Nature **406**: 731–734

Pires MV, Pereira Júnior AA, Medeiros DB, Daloso DM, Pham PA, Barros KA, Engqvist MKM, Florian A, Krahnert I, Maurino VG, et al (2016) The influence of alternative pathways of respiration that utilize branched-chain amino acids following water shortage in *Arabidopsis*. Plant Cell & Environment **39**: 1304–1319

Qin L, Deng Y, Zhang X, Tang L, Zhang C, Xu S, Wang K, Wang M, Zhang X, Su M, et al (2024) Mechanistic insights into phosphoactivation of SLAC1 in guard cell signaling. Proc Natl Acad Sci USA **121**: e2323040121

Rasulov B, Talts E, Bichele I, Niinemets Ü (2018) Evidence That Isoprene Emission Is Not Limited by Cytosolic Metabolites. Exogenous Malate Does Not Invert the Reverse Sensitivity of Isoprene Emission to High [CO_2]. Plant Physiol **176**: 1573–1586

Reiss H-D, Herth W (1985) Nifedipine-sensitive calcium channels are involved in polar growth of lily pollen tubes. Journal of Cell Science **76**: 247–254

Sasaki T, Ariyoshi M, Yamamoto Y, Mori IC (2022) Functional roles of ALMT-type anion channels in malate-induced stomatal closure in tomato and Arabidopsis. Plant Cell & Environment **45**: 2337–

2350

Sasaki T, Mori IC, Furuichi T, Munemasa S, Toyooka K, Matsuoka K, Murata Y, Yamamoto Y (2010) Closing Plant Stomata Requires a Homolog of an Aluminum-Activated Malate Transporter. Plant and Cell Physiology **51**: 354–365

Schroeder JI, Allen GJ, Hugouvieux V, Kwak JM, Waner D (2001) GUARD CELL SIGNAL TRANSDUCTION. Annu Rev Plant Physiol Plant Mol Biol **52**: 627–658

Schwartz A, Ilan N, Schwarz M, Scheaffer J, Assmann SM, Schroeder JI (1995) Anion-Channel Blockers Inhibit S-Type Anion Channels and Abscisic Acid Responses in Guard Cells. Plant Physiol **109**: 651–658

Sweetman C, Deluc LG, Cramer GR, Ford CM, Soole KL (2009) Regulation of malate metabolism in grape berry and other developing fruits. Phytochemistry **70**: 1329–1344

Tan Y-Q, Yang Y, Shen X, Zhu M, Shen J, Zhang W, Hu H, Wang Y-F (2023) Multiple cyclic nucleotide-gated channels function as ABA-activated Ca^{2+} channels required for ABA-induced stomatal closure in Arabidopsis. The Plant Cell **35**: 239–259

Tang R-H, Han S, Zheng H, Cook CW, Choi CS, Woerner TE, Jackson RB, Pei Z-M (2007) Coupling Diurnal Cytosolic Ca^{2+} Oscillations to the CAS-IP_3 Pathway in *Arabidopsis*. Science **315**: 1423–1426

Trauelsen M, Hiron TK, Lin D, Petersen JE, Breton B, Husted AS, Hjorth SA, Inoue A, Frimurer TM, Bouvier M, et al (2021) Extracellular succinate hyperpolarizes M2 macrophages through SUCNR1/GPR91-mediated Gq signaling. Cell Reports **35**: 109246

Trauelsen M, Rexen Ulven E, Hjorth SA, Brvar M, Monaco C, Frimurer TM, Schwartz TW (2017) Receptor structure-based discovery of non-metabolite agonists for the succinate receptor GPR91.

627 Molecular Metabolism **6**: 1585–1596

628 **Urano K, Maruyama K, Ogata Y, Morishita Y, Takeda M, Sakurai N, Suzuki H, Saito K, Shibata**

629 **D, Kobayashi M, et al** (2009) Characterization of the ABA-regulated global responses to dehydration

630 in Arabidopsis by metabolomics. The Plant Journal **57**: 1065–1078

631 **Vahisalu T, Kollist H, Wang Y-F, Nishimura N, Chan W-Y, Valerio G, Lamminmäki A, Brosché**

632 **M, Moldau H, Desikan R, et al** (2008) SLAC1 is required for plant guard cell S-type anion channel

633 function in stomatal signalling. Nature **452**: 487–491

634 **Van Kirk CA, Raschke K** (1978) Release of Malate from Epidermal Strips during Stomatal Closure.

635 Plant Physiol **61**: 474–475

636 **Wada H, Shackel KA, Matthews MA** (2008) Fruit ripening in Vitis vinifera: apoplastic solute

637 accumulation accounts for pre-veraison turgor loss in berries. Planta **227**: 1351–1361

638 **Wang X-Q, Ullah H, Jones AM, Assmann SM** (2001) G Protein Regulation of Ion Channels and

639 Abscisic Acid Signaling in *Arabidopsis* Guard Cells. Science **292**: 2070–2072

640 **Wang Y-F, Munemasa S, Nishimura N, Ren H-M, Robert N, Han M, Puzõrjova I, Kollist H, Lee**

641 **S, Mori I, et al** (2013) Identification of Cyclic GMP-Activated Nonselective Ca^{2+}-Permeable Cation

642 Channels and Associated *CNGC5* and *CNGC6* Genes in Arabidopsis Guard Cells. Plant Physiology

643 **163**: 578–590

644 **Yang Y, Tan Y-Q, Wang X, Li J-J, Du B-Y, Zhu M, Wang P, Wang Y-F** (2024) OPEN STOMATA

645 1 phosphorylates CYCLIC NUCLEOTIDE-GATED CHANNELs to trigger Ca^{2+} signaling for abscisic

646 acid-induced stomatal closure in Arabidopsis. The Plant Cell **36**: 2328–2358

647 **Ye W, Munemasa S, Shinya T, Wu W, Ma T, Lu J, Kinoshita T, Kaku H, Shibuya N, Murata Y**

648 (2020) Stomatal immunity against fungal invasion comprises not only chitin-induced stomatal closure

but also chitosan-induced guard cell death. Proc Natl Acad Sci USA **117**: 20932–20942

Zhang W, Jeon BW, Assmann SM (2011) Heterotrimeric G-protein regulation of ROS signalling and calcium currents in Arabidopsis guard cells. Journal of Experimental Botany **62**: 2371–2379

Figure legends

Figure 1. Metabolome analysis in grapevine leaves during dehydration treatment.

A) PCA score plot of metabolomic datasets colored by the time of dehydration stress as clusters. Dots represent biological replicates. Ellipse display 95% confidence regions of each cluster.

B) Relative ABA levels. Fold changes were normalized to the values of 0 h. Data are the mean ± SE.

C) Volcano plot for the differential metabolites. Red and green dots mark the metabolites with significantly increased and decreased level in 0 h versus 24 h, respectively. Upregulated metabolites are defined VIP >1, $\log_2$(Fold change) ≥1 and P-value >0.05, downregulated metabolites are defined VIP >1, $\log_2$(Fold change) ≤−1 and P-value >0.05. P-value was calculated by Welch's t-test.

D) Categorization of the differential metabolites in **C)**. Upper panel shows upregulated metabolites, and lower panel shows downregulated metabolites.

E) Relative TCA cycle metabolite levels at different time points. Heat maps represent $\log_2$(Fold change). Fold changes were normalized to the values of 0 h. Data were obtained from three independent biological replicates. Abbreviations: F6P, fructose-6-phosphate; F1,6BP, fructose 1,6-bisphosphate;

GADP, glyceraldehyde 3-phosphate; 3PG, 3-phosphoglycerate; PEP, phosphoenolpyruvate; Pyr, pyruvate; Cit, citrate; *cis*-Aco, *cis*-aconitate; Isocit, isocitrate; Keto, α-ketoglutarate; Suc, succinate; Fum, fumarate; Mal, malate; Oxal, oxalacetate; Ser, serine; Trp, tryptophan; Tyr, tyrosine; Phe, phenylalanine; Val, valine; Leu, leucine; Ile, isoleucine; Thr, threonine; Asp, aspartate; Asn, asparagine; Met, methionine; Lys, lysine; Glu, glutamate; Gln, glutamine; His, histidine; Pro, proline; Arg, arginine; GABA, γ-aminobutyrate.

Figure 2. Ca^{2+} response to TCA cycle metabolites in guard cells.

A and **B)** Representative traces of fluorescence emission ratios (535/480 nm) in *A. thaliana* guard cells expressing the Ca^{2+} sensor Yellow Cameleon 3.6. Grey bars indicate the time point when treatment was applied. The guard cells were treated with TCA cycle metabolites 3 min after the measurement.

C and **D)** Percentage of number of guard cells showing different numbers of transient $[Ca^{2+}]_{cyt}$ increases. An increase in $[Ca^{2+}]_{cyt}$ is defined by an increase in fluorescence ratio by ≥0.1 U from the baseline ratio. Data were obtained from Mock (25), Isocit (16) for **C)**; Mock (51 guard cells), Suc (31), Fum (28), Mal (44) Oxal (27), Keto (28), Cit (30), cis-Aco (29), Ace (33), Pyr (33), Mal+La^{3+} (21) for **D)**. Asterisks and taggers indicate statistical significances based on Fisher's exact test, P ≤0.05. Abbreviations: Isocit, isocitrate; Suc, succinate; Fum, fumarate; Mal, malate; Oxal, oxalacetate; Keto, α-ketoglutarate; Cit, citrate; cis-Aco, *cis*-aconitate; Ace, acetate; Pyr, pyruvate.

Figure 3. The negative currents of Xenopus oocytes expressing VvSLAC1F440A.

688 **A to D)** A ribbon model of a VvSLAC1 protomer. A top view of the promoter is shown **A)**, and side
689 views are shown **B to D)**. The VvSLAC1 structure model is displayed in red and the AtSLAC1 structure
690 is displayed in green for comparison. The side chain of Phe 440 of VvSLAC1 is shown in magenta and
691 Phe 450 of AtSLAC1 is shown in blue. The pore is shown as solid surface.

692 **E)** Representative whole-cell negative current recordings in Xenopus oocytes expressing
693 VvSLAC1F440A. The voltage pulse was commanded to clamp the membrane potential from +60 mV
694 to −160 mV in −20 mV steps for 2.5 seconds with a holding potential of 0 mV.

695 **F)** Average steady-state current–voltage curves of whole-cell negative current recordings.

696 **G)** Average steady-state negative currents at −160 mV in **C)**. Data are the mean ± SE (n = 12 for
697 VvSLAC1; n = 7 for VvSLAC1F440A). Different letters indicate statistical significances based on
698 Student's *t*-test, $P < 0.05$.

699

700 **Figure 4.** VvSLAC1 activity in the presence of TCA cycle metabolites.

701 **A)** Representative whole-cell negative current traces during perfusion with TCA cycle metabolites in
702 water-injected Xenopus oocytes. The voltage pulse was commanded to clamp the membrane potential
703 at −120 mV. Grey regions indicate metabolite perfusion and white regions indicate washout.

704 **B)** Average of relative currents. The currents were normalized to the mock-treated current. Data were
705 obtained from six oocytes per condition. Data are the mean ± SE.

706 **C)** Representative whole-cell negative current traces during perfusion with TCA cycle metabolites in

Xenopus oocytes expressing VvSLAC1F440A.

D) Average of relative currents. Data are the mean ± SE (n = 5 for VvSLAC1; n = 6 for VvSLAC1F440A).

E) Average steady-state current–voltage curves of whole-cell negative current recordings in bathing solution supplemented with TCA cycle metabolites. The voltage pulse was commanded to clamp the membrane potential from +60 mV to −160 mV in −20 mV steps for 2.5 seconds with a holding potential of 0 mV.

F) Average steady-state negative currents at −160 mV in **E)**. Data are the mean ± SE. Data were obtained from four oocytes per condition. Different letters indicate statistical significances based on one-way ANOVA with Tukey's HSD test, $P < 0.05$. Abbreviations: Suc/S, succinate; Fum/F, fumarate; Mal/M, malate; Oxal/O, oxalacetate; Keto/K, α-ketoglutarate; Cit, citrate; Isocit/I, isocitrate; Cis, *cis*-aconitate; Ace/A, acetate; Pyr/P, pyruvate.

Figure 5. Malate-induced stomatal closure is mediated by anion channels and second messengers.

A and **B)** Effects of TCA cycle metabolites on stomatal aperture in **A)** *V. vinifera* or **B)** *A. thaliana* leaves. Data are the mean ± SE. Different letters indicate statistical significances based on one-way ANOVA with Tukey's HSD test, $P < 0.05$.

C to **I)** Effects of inhibitors on malate-induced stomatal closure in **C**, **D** and **H)** *V. vinifera* or **E** to **G**, **I)** *A. thaliana* leaves. Averages of stomatal apertures from four independent experiments (n = 4) are shown. Data are the mean ± SE. Different letters indicate statistical significances based on two-way ANOVA

727 with Tukey's HSD test, $P < 0.05$. Abbreviations: Suc, succinate; Fum, fumarate; Mal, malate; Oxal,
728 oxalacetate; Keto, α-ketoglutarate; Cit, citrate; Isocit, isocitrate; cis-Aco, *cis*-aconitate; Ace, acetate; Pyr,
729 pyruvate; Nif, nifedipine; Nic, nicotinamide.

730

731 **Figure 6.** Malate-induced $[Ca^{2+}]_{cyt}$ elevations are mediated by cADPR, cAMP and IP_3.

732 **A)** Representative traces of fluorescence emission ratios (535/480 nm) in *A. thaliana* guard cells
733 expressing the Ca^{2+} sensor Yellow Cameleon 3.6. Grey bar indicates the time point when treatment was
734 applied. The guard cells were treated with malate 3 min after the measurement. Inhibitors were added 5
735 min before starting imaging.

736 **B)** Percentage of number of guard cells showing different numbers of transient $[Ca^{2+}]_{cyt}$ increases. An
737 increase in $[Ca^{2+}]_{cyt}$ is defined by an increase in fluorescence ratio by ≥0.1 U from the baseline ratio.
738 Data were obtained from Mock (10 guard cells), Mal (12), +Nicotinamide (13), +Alloxan (10),
739 +Neomycin (15), +SHAM (12). Asterisks indicate statistical significances based on Fisher's exact test,
740 $P \leq 0.05$.

741

742 **Figure 7.** Malate signaling is mediated by G-proteins.

743 **A and B)** Effects of G-protein inhibitors on malate-induced stomatal closure in **A)** *V. vinifera* or **B)** *A.*
744 *thaliana* leaves.

745 **C)** Effects of *gpa1* and *agb1* mutation on malate-induced stomatal closure. Averages of stomatal
746 apertures from four independent experiments (n = 4) are shown. Data are the mean ± SE. Different letters

747 indicate statistical significances based on two-way ANOVA with Tukey's HSD test, $P < 0.05$.

748 **D)** Representative traces of fluorescence emission ratios (535/480 nm) in *A. thaliana* guard cells
749 expressing the Ca^{2+} sensor Yellow Cameleon 3.6. Grey bar indicates the time point when treatment was
750 applied. The guard cells were treated with malate 5 min after the measurement. Inhibitors were added 5
751 min before starting imaging.

752 **E)** Percentage of number of guard cells showing different numbers of transient $[Ca^{2+}]_{cyt}$ increases. An
753 increase in $[Ca^{2+}]_{cyt}$ is defined by an increase in fluorescence ratio by ≥0.1 U from the baseline ratio.
754 Data were obtained from Mock (34 guard cells), Mal (32), +GDP β S (33). Asterisks indicate statistical
755 significances based on Fisher's exact test, $P \leq 0.05$.

756 **F)** Effects of GDPβS on malate-induced ROS production in *A. thaliana* guard cells. The ROS-sensitive
757 dye, 2',7'-dichlorodihydrofluorescein diacetate (H_2DCF-DA) was used for ROS detection in guard cells.
758 Fluorescence intensity was normalized to mock value in water.

759 **G)** Effects of *gpa1* and *agb1* mutation on malate-induced ROS production in *A. thaliana* guard cells.
760 Fluorescence intensity was normalized to mock value in WT. Averages from three independent
761 experiments (n = 3) are shown. Data are the mean ± SE. Different letters indicate statistical significances
762 based on two-way ANOVA with Tukey's HSD test, $P < 0.05$.

763 **H)** A proposed working model for malate signaling.

Fig. 1 Metabolome analysis in grapevine leaves during dehydration treatment.

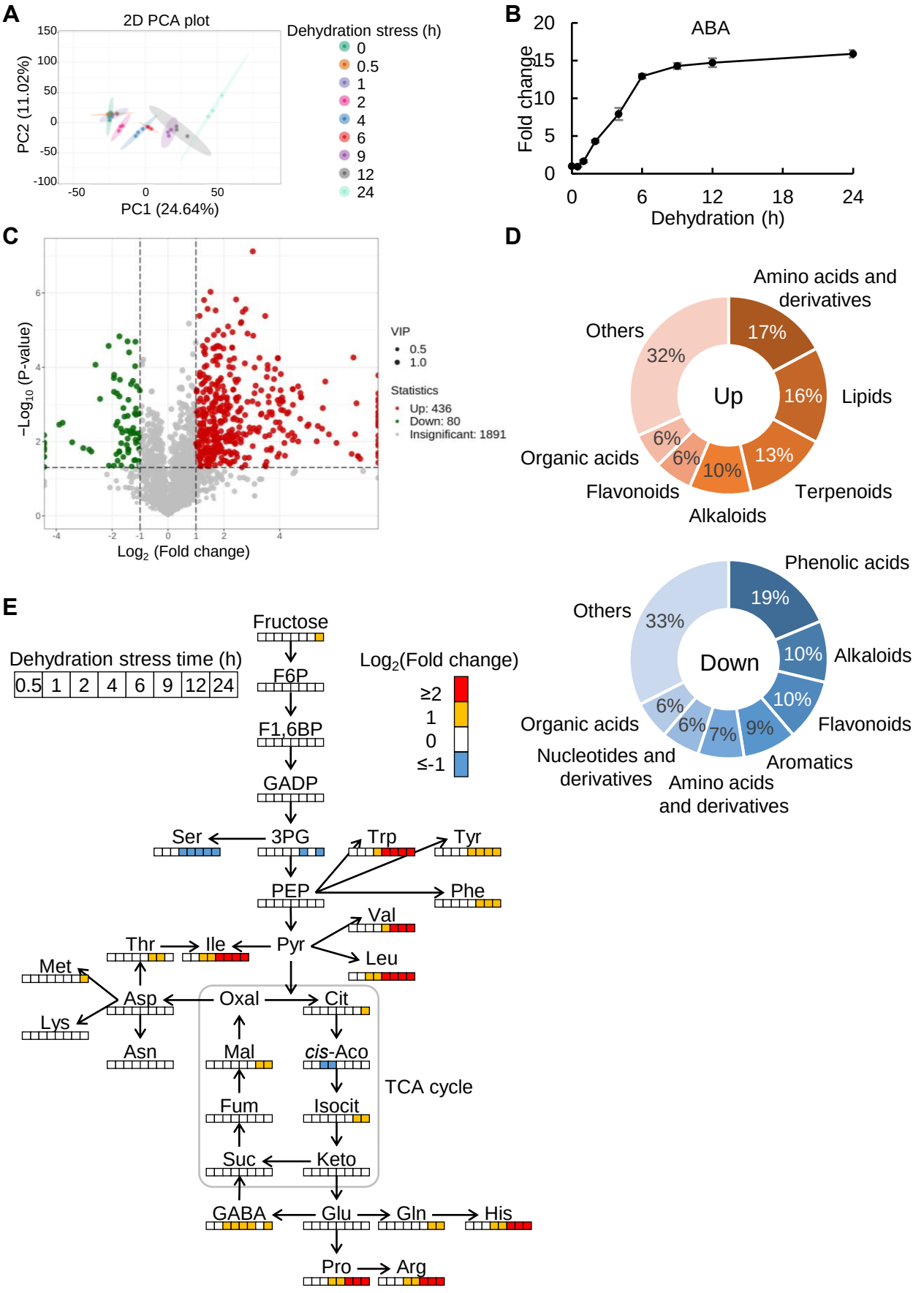

Fig. 2 Ca^{2+} response to TCA cycle metabolites in guard cells.

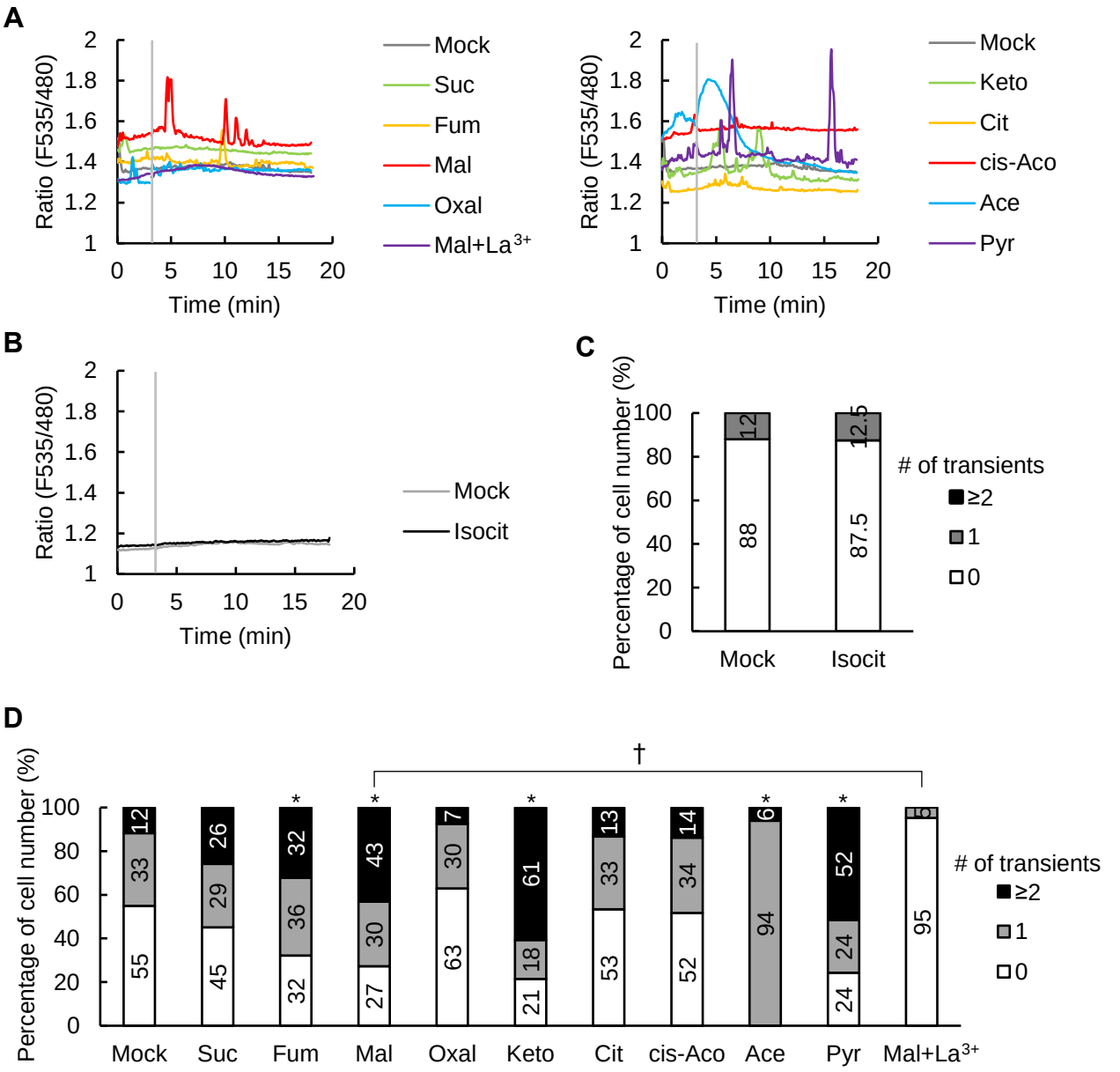

Fig. 3 The negative currents of Xenopus oocytes expressing VvSLAC1F440A.

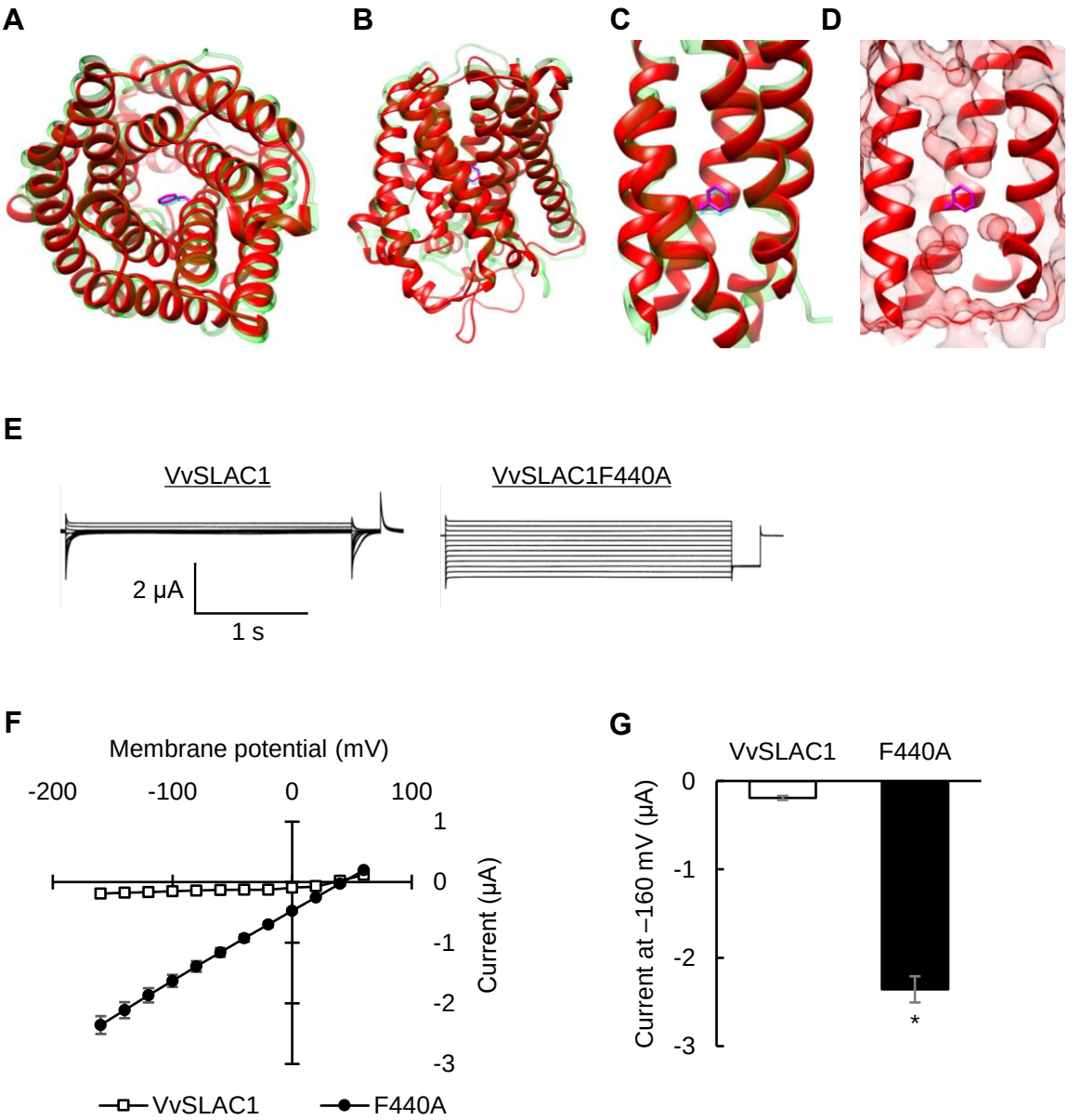

Fig. 4 VvSLAC1 activity in the presence of TCA cycle metabolites.

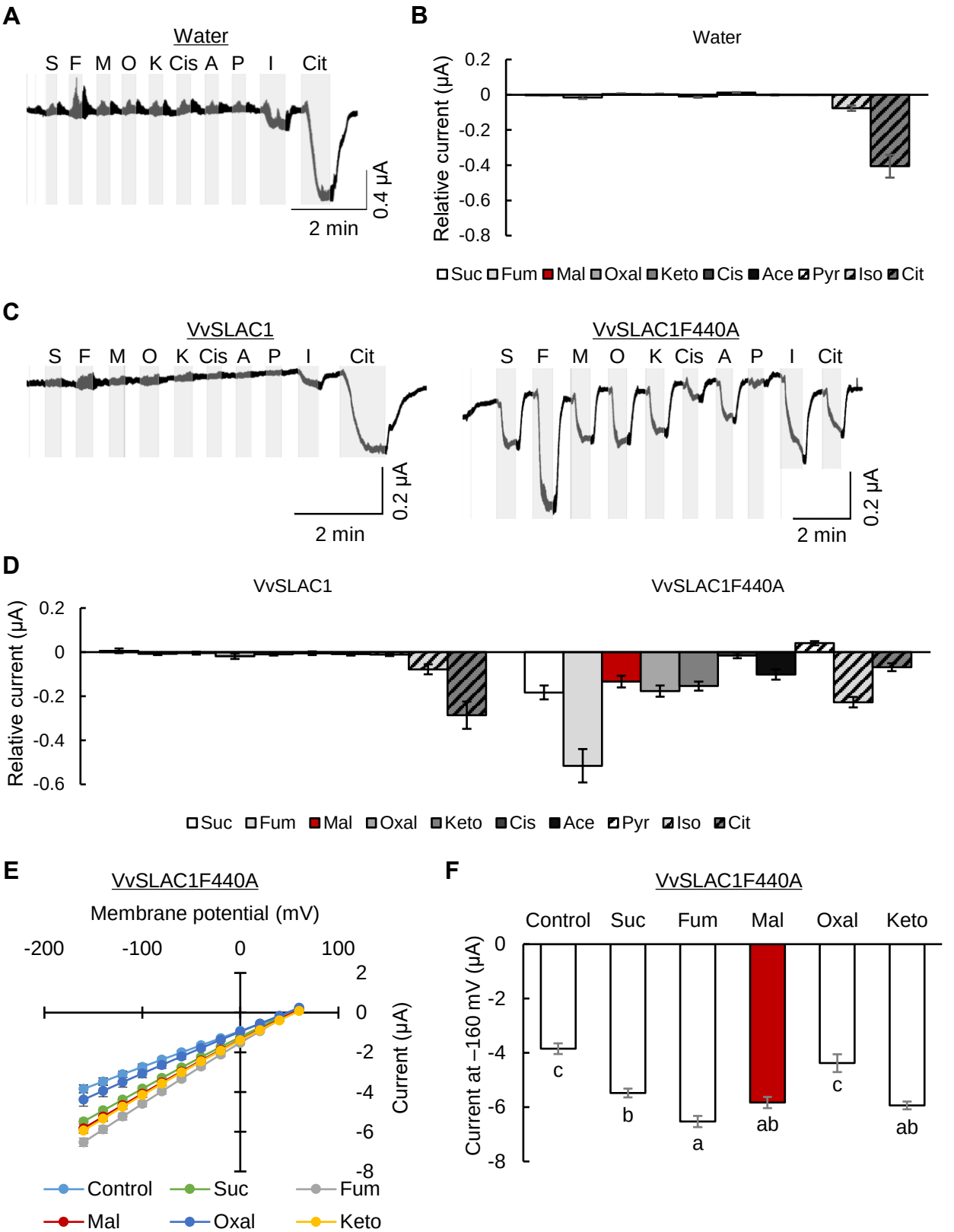

Fig. 5 Malate-induced stomatal closure is mediated by anion channels and second messengers.

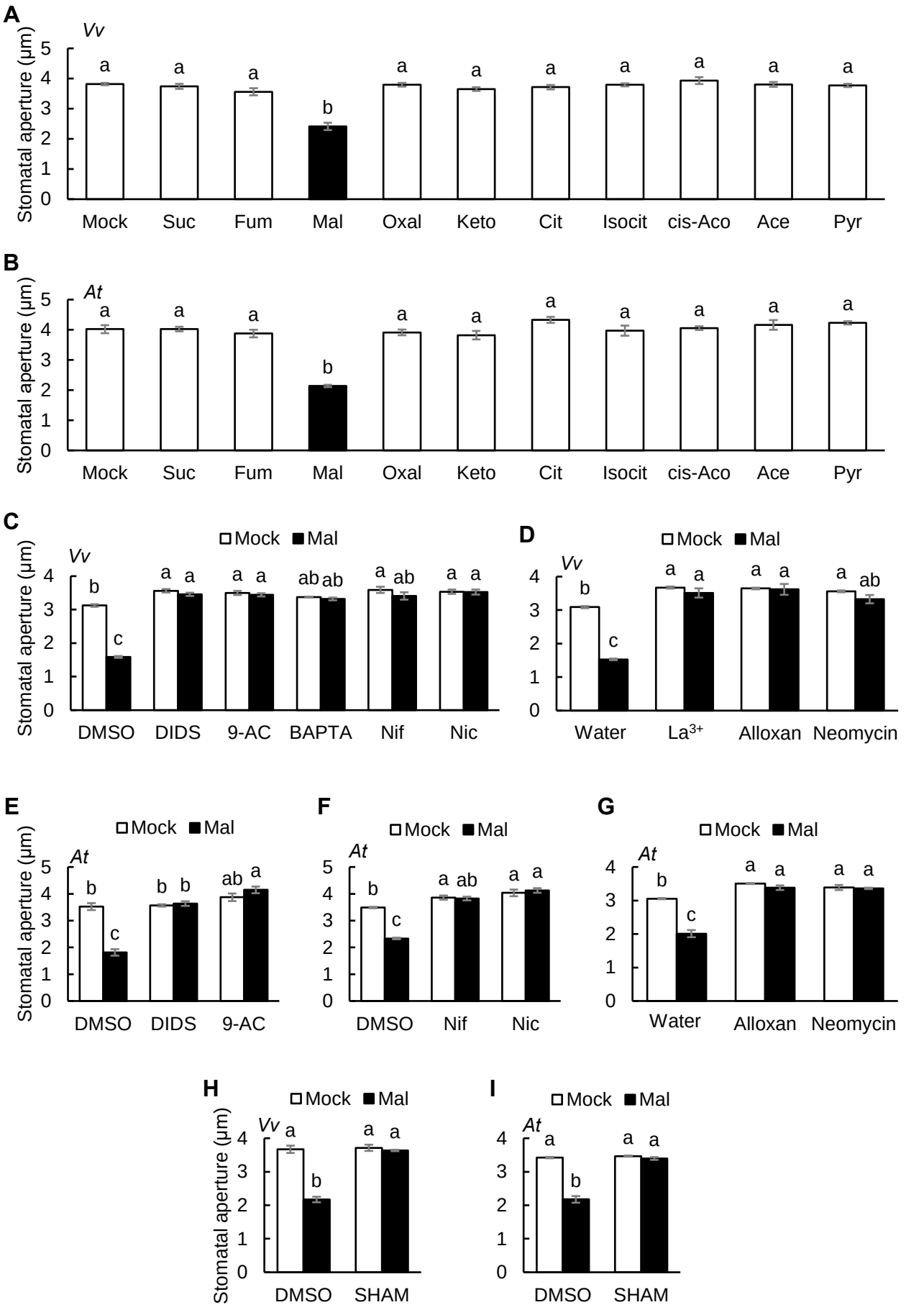

Fig. 6 Malate-induced $[Ca^{2+}]_{cyt}$ elevations are mediated by cADPR, cAMP and IP_3.

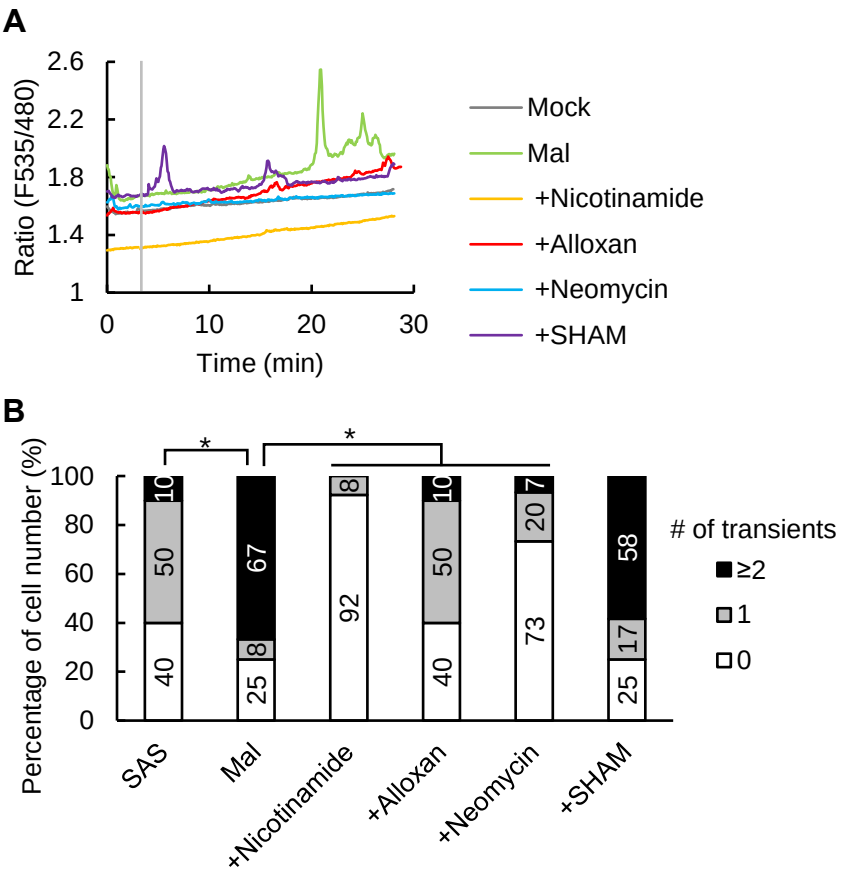

Fig. 7 Malate signaling is mediated by G-proteins.